Organic & Biomolecular Chemistry

Accepted Manuscript

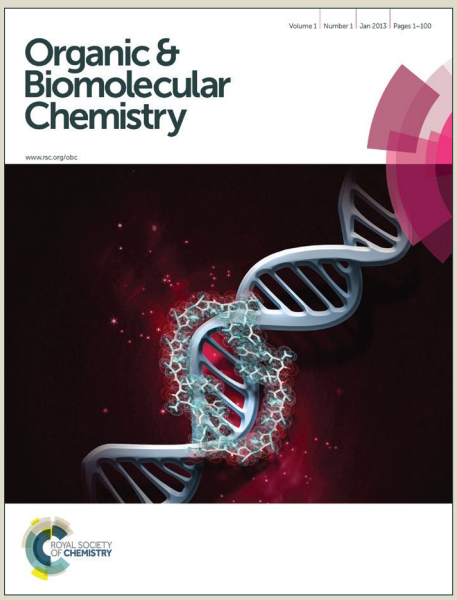

ROYAL SOCIETY OF CHEMISTRY

www.rsc.org/obc

Journal Name

RSCPublishing

ARTICLE

Recognition of bio-relevant dicarboxylate anions by an azacalix[2]arene[2]triazine derivative decorated with urea moieties

Miguel Santos,[a,b] Igor Marques,[a] Sílvia Carvalho,[a] Cristina Moiteiro*[b] and Vítor Félix*[a]

Cite this: DOI: 10.1039/xoxxoooooox

Received ooth January 2012,
Accepted ooth January 2012

DOI: 10.1039/xoxxoooooox

www.rsc.org/

A new dichloroazacalix[2]arene[2]triazine receptor (**1**) with two chiral urea binding moieties is reported. The binding affinity of this macrocycle was evaluated by ^{1}H NMR titrations in $CDCl_3$ for the dicarboxylate anions oxalate (ox^{2-}), malonate (mal^{2-}), succinate (suc^{2-}), glutarate (glu^{2-}), diglycolate (dg^{2-}), fumarate (fum^{2-}), maleate ($male^{2-}$), and (*R*,*R*)- and (*S*,*S*)-tartarate ($tart^{2-}$) enantiomers. Among the first five linear anions, the higher association constants were calculated for the larger anions glu^{2-} and dg^{2-} and for the smallest anion ox^{2-}, with K_{ass} values following the sequence dg^{2-} > glu^{2-} > ox^{2-} > suc^{2-} > mal^{2-}. Although the high binding affinity of **1** for both $tart^{2-}$ enantiomers, no enantioselectivity was observed. By contrast, K_{ass} for fum^{2-} is *ca*. 8.9 times greater than for $male^{2-}$, showing the selectivity of **1** for the *trans* isomer. These binding preferences were further elucidated by theoretical methods. Molecular dynamics simulations showed that the linear anions are lodged between both pendant arms and that each anion can assume two distinct binding poses, with one or two carboxylate groups establishing intermittent hydrogen bonds with both urea binding units. On another hand, the recognition of $male^{2-}$ ensues in an alternative scenario, characterised by the interaction between a carboxylate group and a single urea binding unit, mirroring the lower experimental binding affinity relatively to fum^{2-}. A linear increase of the receptor's $N_{urea}\cdots N_{urea}$ and the anions' $^{-}O_2C\cdots CO_2^{-}$ distances, *versus* experimental K_{ass} was established for mal^{2-}, suc^{2-}, glu^{2-} and dg^{2-} associations, indicating that the match between these two distances determines the anion binding strength. The affinity for ox^{2-} was associated with the most negative values of electrostatic potential positioned near of carboxylate groups.

Introduction

Dicarboxylate anions are an important target in supramolecular chemistry[1] due to their role in crystal engineering,[2] medicinal chemistry, molecular biology and food chemistry.[3] Concerning their biological relevance, it is worth mentioning that both succinic and fumaric acids play major roles in the Krebs cycle.[4] In addition, the succinic acid is also important in the membrane electron transport chain, thus linking both fundamental cellular processes through the succinate dehydrogenase.[5] This membrane enzyme can be inhibited by other dicarboxylic acids, such as the malonic and maleic acids,[6] while the metabolism of the fumaric acid to malic acid in the Krebs cycle can be inhibited by the D-tartaric acid.[7] The inhibition of either steps leads to the dysfunction of the Krebs cycle, which is related to several disorders, including paragangliomas, renal cancer, uterine leiomyomas, autism and fibromyalgia, among others.[7-8] Furthermore, the glutaric acid results from the metabolism of aminoacids such as lysine or tryptophan. An excess of glutaric acid, due to a deficiency of glutaryl-CoA dehydrogenase, leads to glutaric aciduria, which mainly affects the brain.[9] Moreover, the bodily oxalic acid can result from the Krebs cycle or from the diet, through the metabolism of larger carboxylic acids,[10] and the accumulation of this biogenic substrate in the body can lead to several diseases, such as kidney stones.[10b] Also, dicarboxylic acids have been applied in the formulation of drug delivery systems, as illustrated by the following examples: enalapril maleate,[11] metoprolol tartrate and metoprolol succinate,[12] escitalopram oxalate,[13] and quetiapine fumarate.[14] Given the key roles of several dicarboxylate anions in the maintenance of biological processes, the design of receptors able to selectively recognize these anions *via* intermolecular interactions, such as hydrogen bonds, anion$\cdots\pi$ interactions or halogen bonds is of paramount importance and has received a renewed attention along the last years.[15]

The classical calix[*n*]arenes are one of the macrocyclic platforms that have been widely used to build a plethora of synthetic receptors decorated with binding moieties, yielding almost rigid structures with powerful affinities for different anionic guests.[16] Alongside with the calix[*n*]arene chemistry outcomes, recent achievements on the synthesis of heteroatom bridged calix(hetero)aromatics have made these macrocycles very attractive platforms for the design of innovative anion receptors.[17] For instance, the dichlorocalix[2]arene[2]triazine molecules are endowed with inherent anion affinity given by the electron-deficient triazine moieties promoting anion···π interactions, as recently reported for dichlorotetraoxacalix[2]arene[2]triazine, which binds the inorganic anions Cl^-, Br^-, NO_3^-, NCS^-, BF_4^- and PF_6^- within the 1,3-alternate cavity.[18] Moreover, Wang *et al*., in their seminal work, reported a high yielding stepwise synthesis of calix[2]arene[2]triazine macrocycles with phenyl and triazine moieties bridged by nitrogen and/or oxygen atoms.[19] These molecules show distinct conformational properties rendered by the conjugation of the aromatic and heteroaromatic rings through the heteroatom bridges, leading to a fine-tuned cavity in response to anion addition. On the other hand, the calix[2]arene[2]triazine platforms can easily be used to anchor substituents with binding units, as recently shown by our group with the functionalization of dichlorotetraazacalix[2]arene[2]triazine on the phenyl rings as well as on the nitrogen bridging atoms. Firstly, we delivered dichlorotetraazacalix[2]arene[2]triazines substituted in one or both phenyl rings with L-alanine residues.[20] The receptors with two amino acid units are able to bind the selected aromatic and aliphatic mono- and dicarboxylate anions in a cooperative fashion using the amide groups from both arms. By contrast, the recognition of the same anionic substrates by the receptors with a single amino-acid binding unit also involves at least one N-H bridging unit. Afterwards, undecorated tetraazacalix[2]arene[2]triazine derivatives with chlorine or N,N′-dialkyl substituted triazine rings were functionalised on the nitrogen bridges with four carboxymethyl arm, which were further hydrolysed yielding receptors with coordination ability for Cu^{2+}.[21]

Following our previous efforts on the research for new carboxylate anion receptors, we herein report the synthesis of a tetraazacalix[2]arene[2]triazine-based macrocycle armed with chiral substituents containing urea motifs attached to the phenyl rings, as depicted in Scheme 1. The urea binding motifs were selected due to their acidic character and geometry, which enable them to establish multiple and highly stabilized N-H hydrogen bonds with anion guests with different geometries.[15d, 15f, 15i, 22] Subsequently the binding ability of tetraazacalix[2]arene[2]triazine **1** was evaluated for a wide series of biologically relevant dicarboxylate anions, also shown in Scheme 1. The selective recognition of enantiomeric carboxylate anions, as well as of geometric isomers, was also investigated. These studies were conducted by ^{1}H NMR titration experiments in $CDCl_3$. Molecular dynamics simulations were also performed to elucidate, at the atomistic level, the recognition process of selected carboxylate anions. This theoretical study was complemented by electrostatic calculations on the receptor and anions.

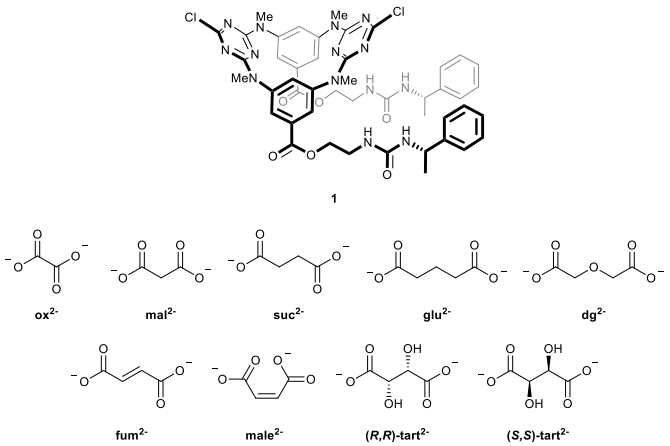

Scheme 1

Results and discussion

Molecular design and synthesis of 1

Generally the azacalix[2]arene[2]triazine scaffold displays an 1,3-alternate conformational shape that spatially guides binding entities inserted at either *meta*- or *ortho*- positions of both phenyl rings for putative and cooperative anion recognition.[17d] Furthermore, as aforementioned, the anion affinity can be enhanced by the inherent electron deficiency character of the unsubstituted dichloroazacalix[2]arene[2]triazine macrocycle. Based on these structural features we devised macrocyle **1** (Scheme 1) to recognize a wide series of carboxylate anions. This molecule contains urea binding motifs attached to the *meta*- position of both phenyl rings through ethanolamine spacers. This linker was selected to allow the carboxylates' recognition between the two binding moieties and in the vicinity of the dichloroazacalix[2]arene[2]triazine's cavity. Furthermore, the four nitrogen-bridging atoms of **1** are strategically methylated in order to direct the anion recognition to the urea binding units, as well as to increase its solubility in organic media such as $CHCl_3$.

We primarily aimed for the synthesis of the appended urea moieties and followed *en route* to the disubstituted macrocycles as depicted in Scheme 2. All compounds, apart from **5** and **6**, were fully characterised by NMR and IR spectroscopies and complemented by MS, as described in the experimental section. The binding fragment **3** was prepared by reacting (*S*)-(*α*)-methylbenzyl isocyanate (**2**) with ethanolamine in chloroform with 93% yield after recrystallization from ethyl acetate. Subsequently, the intermediate **4** was obtained by coupling 3,5-dinitrobenzoyl chloride with **3** in 87% yield.

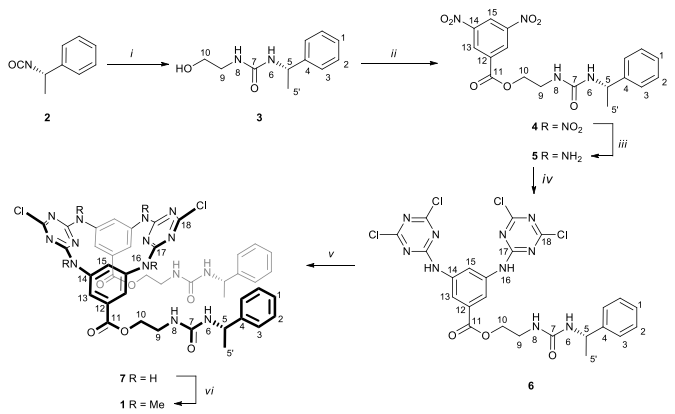

Reagents and conditions: i. ethanolamine, $CHCl_3$, rt, 20h, 93%; *ii.*3,5-dinitrobenzoyl chloride, THF, K_2CO_3, rt, 18h, 87%; *iii.* H_2, Pd/C(en) 10%, EtOH, ≈50 psi, rt, 2h, quantitive yield.; *iv.*cyanuric chloride, DIPEA, THF, -20 °C → rt, 2h; *v.* **5**, DIPEA, acetone, 56 °C, 7d, 51%; *vi.* MeI, Cs_2CO_3, MeCN, rt, 18h, 73%.

Scheme 2.

The first piece of the azacalix[2]arene[2]triazine skeleton, the intermediate **5**, was obtained from the quantitative reduction of the nitro groups with 10% Pd/C(en).[23] Afterwards, the linear trimer **6** was prepared by the reaction of **5** and two highly reactive cyanuric chloride units in THF following the procedure reported by Wang *et al*.[19] Despite the fact that we were unable to completely purify this compound, the introduction of the two triazine moieties was confirmed by a singlet at δ 11.00 ppm in the ^{1}H NMR (DMSO-d_6),[19] which is consistent with the presence of two NH bridging protons. The synthesis proceeded with macrocyclization of **6** with another unit of **5** leading to the intermediate macrocycle **7** in 51% yield following slightly different experimental conditions from the ones originally reported by Wang *et al*,[19] and already published by us.[20-21] The formation of this azacalix[2]arene[2]triazine derivative was confirmed by the singlet at δ 10.19 ppm in the ^{1}H NMR spectrum that integrates the four N-H bridging protons. Also, the ^{13}C APT NMR spectrum shows the quaternary signal from the triazine's C-N and C-Cl groups at δ 164.6 and 168.3 ppm, respectively. Both NMR spectra show only one set of resonances, in agreement with a C_2 symmetry witnessed at 298 K in the NMR time scale.[19] The obtained HRMS-ESI spectrum was also consistent with the formation of **7**, showing the $[M+H]^+$ ion peak at *m/z* 907.26710 and a characteristic ^{35}Cl/^{37}Cl isotopic distribution for the two chlorine atoms in the molecule.[24]

The last step of our synthetic approach comprised the full methylation of the nitrogen bridges of **7** with MeI, affording the target $(NMe)_4$-azacalix[2]arene[2]triazine **1**. However, this reaction was far from trivial so different solvents (THF, MeCN, DMF), bases (K_2CO_3, Cs_2CO_3, DIPEA) and reaction temperatures had to be investigated. Indeed, we realized that the highest consumption of the starting material, though never complete, occurred only when 16 equivalents of Cs_2CO_3 in MeCN at 42°C were employed. Furthermore, when more than 4.2 equivalents of methylating agent were used, a mixture of compounds containing five or six methyl groups was obtained as shown by ESI mass spectrometry. The unreacted intermediate **7** was further subjected to identical reaction conditions, up to four times, totalizing 73% yield of transformation to **1**. In addition, other reaction conditions of Eschweiler–Clarke's[25] and $(MeO)_2CO$+DBU[26] were experimented but lacked reactivity and failed to provide the target compound. The ^{1}H NMR spectrum recorded at room temperature confirmed the introduction of the four methyl groups by the presence of a singlet at δ 3.38 ppm, which integrated for 12 protons. The four *ortho* protons of the macrocyclic phenyl rings appear at 7.38 ppm as a broad singlet. A further variable-temperature (VT) ^{1}H NMR experiment shows that both signals split into two singlets at 234 K, as depicted in Figures S22-S23. This structural finding is consistent with one of two alternative conformations in solution at low temperature, where the rotation around the C_{Ph}-C=O linkage is hindered. In one conformation (c_1), the two urea arms are directed towards the same triazine ring, while in the second one (c_2) each arm is facing one triazine ring. The latter spatial disposition was observed in the four azacalix[2]arene[2]triazine independent molecules present in the crystal structure of **1** (*vide infra*).

The obtained HRMS-ESI data cements the formation of **1** as the peak at *m/z* 963.33013 is consistent with the $[M+H]^+$ ion, and it shows the characteristic ^{35}Cl/^{37}Cl isotopic distribution for two chlorine atoms in the molecule. The structure of **1** was definitively established by single crystal X-ray diffraction analysis, as follows.

X-Ray crystallography

The azacalix[2]arene[2]triazine **1** crystallized in the chiral space group $P\bar{1}$ from an asymmetric unit composed of four independent molecules (A – D) exhibiting a 1,3-alternate conformation, as illustrated in Figure 1 for **D**. This conformational shape is commonly reported in solid state for aza, azaoxa- and oxacalix[2]arene[2]triazine-based macrocycles.[19-21,27]

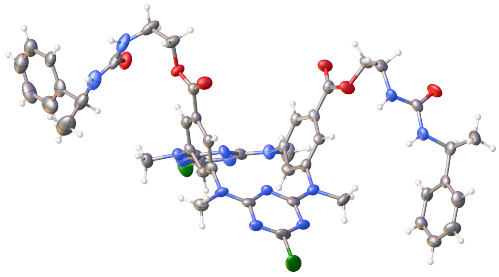

Figure 1. ORTEP diagram of D with thermal ellipsoids drawn at 50% probability level illustrating the 1,3-alternate conformation adopted by the four independent molecules of **1**. The hydrogen, carbon, oxygen, nitrogen and chlorine atoms are shown in white, grey, red, blue and green, respectively.

The arms of each one of the molecules assume diametrically opposing spatial orientations with torsion angles between the ester C=O bonds (O=C···C=O) from both arms of 116.8(6), -

115.5(6), 111.4(6) and -112.3(6)° for A, B, C and D, respectively. The chirality of both chiral centres is retained as in the starting material (*S*)-(*α*)-methylbenzyl isocyanate. Actually, these molecules differ from each other mainly on the conformations adopted by the pendant arms, which are determined by a delicate balance between intermolecular interactions, namely hydrogen bonds observed in the crystal packing (*vide infra*) and the conformational freedom given by the ethylene spacers. Therefore, apart from the exocyclic torsion angles associated with the decorating arms, the individual molecules have comparable bond lengths and angles, as illustrated by the dimensions of the C-N_{bridge} and C-N-C_{bridge} bonds at the macrocyclic nitrogen bridges listed in Table 1.

Table 1. Selected bond lengths (Å) and angles (°) for the azacalix[2]arene[2]triazine platform of **1**.

Molecule	A	B	C	D
Bond lengths				
N_{bdg}-C_{Ph} [a)]	1.447(8)	1.445(8)	1.442(8)	1.436(8)
	1.419(8)	1.433(8)	1.441(8)	1.431(8)
	1.435(8)	1.437(8)	1.428(8)	1.443(8)
	1.444(8)	1.427(8)	1.434(8)	1.439(8)
N_{bdg}-C_{tzn} [a)]	1.342(8)	1.345(8)	1.338(8)	1.344(9)
	1.357(8)	1.344(8)	1.343(9)	1.352(9)
	1.341(8)	1.364(7)	1.350(9)	1.323(8)
	1.356(8)	1.344(8)	1.347(9)	1.355(9)
Bond angles				
C_{Ph}-N_{bdg}-C_{tzn} [a)]	122.6(5)	121.6(5)	122.1(5)	121.4(5)
	121.8(5)	122.6(5)	122.8(5)	121.0(6)
	121.8(5)	121.7(5)	120.8(6)	122.5(5)
	121.0(5)	122.3(5)	122.0(5)	121.1(6)
Dihedral angles [b)]				
α	29.4(2)	27.7(2)	24.6(2)	29.1(2)
	25.3(2)	29.2(2)	28.4(2)	30.4(2)
β	72.0(2)	76.1(2)	75.4(2)	75.1(2)
	71.9(2)	68.4(2)	70.0(2)	70.1(2)

[a)] the subscript notation bdg means nitrogen bridging atoms, while Ph and tzn denote the phenyl and triazine rings, respectively. [b)] α and β are defined in the main text.

Table 1 also contains the α and β dihedral angles given by the interception of the N_4 macrocyclic plane, defined by the nitrogen bridging atoms, with the adjacent triazine and phenyl rings, respectively. Both triazine rings are slightly tilted in relation to the N_4 macrocyclic plane by an average α angle of 28.0° calculated for the four independent molecules, while the adjacent phenyl rings are slightly deviated from the perpendicular to the N_4 plane by an average 90-β angle of 17.7°. This structural feature leads to C-$N_{bridges}$ bond lengths for the phenyl rings systematically longer than the corresponding ones for the triazine rings, which is in agreement with the intermediate sp^2/sp^3 hybridation character assumed by the nitrogen bridging atoms within the azacalix[2]arene[2]triazine platform.[19]

In the crystal packing, the four independent molecules are assembled into two alternative layers running along the [100] crystallographic plane, as seen in Figure 2, view *a*). The first one is composed of molecules A and B (layer AB) and the second one by C and D ones (layer CD). Furthermore, in both layers, the corresponding molecules (A and B or C and D) are connected by a 2D network of N-H···O hydrogen bonds between the adjacent urea groups as shown in views *b*) and *c*) of Figure 2. The dimensions of these bonding interactions are gathered in Table S1. In summary, the crystal structure can be described by (AB)(CD)(AB)(CD)… layers packed along the *a* crystallographic direction.

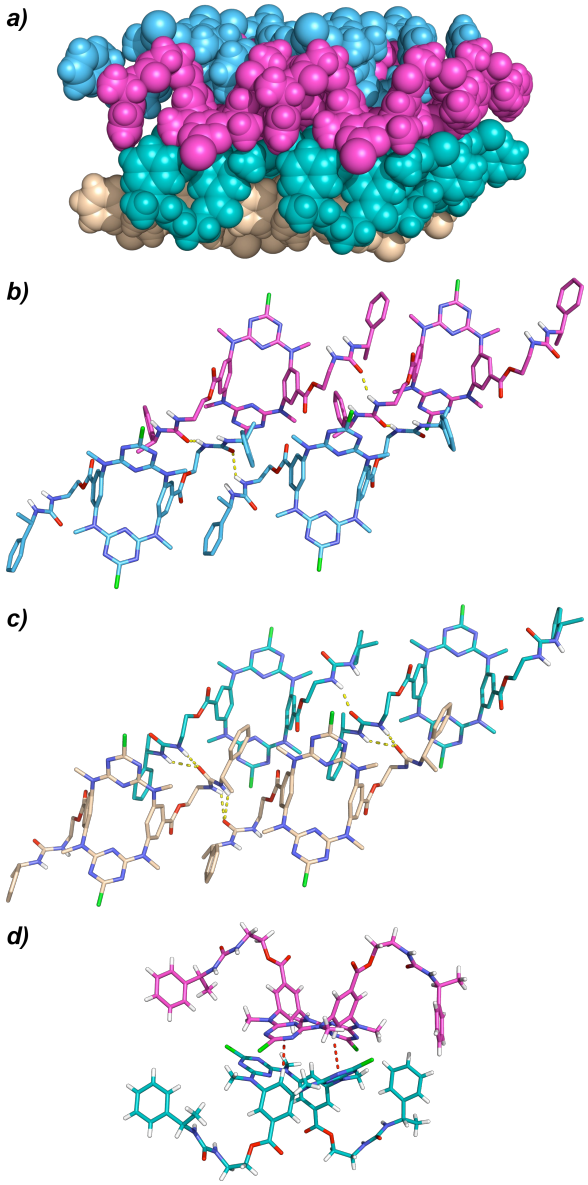

Figure 2. Prominent crystal packing features of **1**: view *a*) CPK representation showing the AB layers alternating with CD ones; views *b* and *c*) 2D networks of N-H···O hydrogen bonds through the AB (*b*) and CD (*c*) layers; view *d*) self-assembling of molecules A and C with their wider rims faced to each other and rotated around 90°;. In *b), c)* and *d),* carbon atoms of A, B, C and D are in light magenta, light blue, teal and wheat, respectively. Hydrogen, oxygen, nitrogen and chlorine atoms are in white, red, blue and green, respectively. In the crystal packing diagram *a*) all atoms are drawn in the colour used for the carbon atoms.

Another interesting structural feature seeming from the crystal structure is the self-assembling of molecules A and C with their wider rims faced to each other and rotated by an angle of

85.11(5)° between the lines defined by the corresponding chlorine atoms (see Figure 2, view *d*). The two phenyl hydrogen atoms of each molecule (A or C), between the nitrogen bridges (CH-15), are directed towards the centre of the wider rim of the neighbouring one. In addition two C-H hydrogen atoms from each one of these molecules are at short distances from the centroids of the electron deficient triazine rings (H···Centroid$_{tzn}$ 2.871 and 3.296 Å) with C-H···Centroid corresponding angles (157.0 and 126.3°) consistent with the existence of CH···π interactions, which can play an important role in the stabilization of this self-assembled arrangement.

Anion recognition studies by ^{1}H NMR

Linear dicarboxylate anions. The binding affinity studies of **1** by ^{1}H NMR spectroscopy began with the linear dicarboxylate anions (as tetrabutylammonium salts) series composed of ox^{2-}, mal^{2-}, suc^{2-} and glu^{2-}, with an increasing number of $(CH_2)_n$ units (n = 0 to 3) linking the carboxylate groups. This rational study permitted to ascertain the optimal chain size of the dicarboxylate anions for the best fitting with the urea binding units of **1**. Moreover, the diglycolate anion (dg^{2-}), analogous to glu^{2-} (see Scheme 1), was included given that it was previously found to be recognised in the solid state by the 1,3-alternate cavity of a azacalix[2]arene[2]triazine derivative containing four carboxymethyl pendant arms on the nitrogen bridges.[21] These experiments were conducted by means of ^{1}H NMR titrations at 298 K, and consisted in recording the variation of the protons' chemical shifts upon the addition of known quantities of substrate to **1**, both in $CDCl_3$ solutions. Downfield variations are expected as the result of putative N-H···O hydrogen bonds established between the receptor urea protons and the carboxylate groups of the substrates, while through-bond polarization effects eventually yield upfield shifts.[28] The evolution of receptors' resonances upon successive addition of 0.1, 0.9, 2.8 and 4.0 equivalents of glu^{2-} is shown in Figure 3. Equivalent spectra for titration experiments of **1** with ox^{2-}, mal^{2-}, suc^{2-} and dg^{2-} anions are plotted along the Figures S25-S28, respectively.

As aforementioned, the binding process of the dicarboxylate anions led to a distinct downfield shift of all NH signals, which is particularly evident for the NH-8 resonance. As illustrated in Figure 3 for the association with glu^{2-}, these signals concomitantly become broader and eventually collapse with the background. The phenyl resonances H-3 also suffer downfield shifts, although with Δδ smaller than 0.089 ppm (see Figure 4), which are consistent with the discrete participation of these protons in the stabilization of all anion complexes.

The downfield variations recorded for the signals from protons H-3 were found to be more consistent with the associative models given that the resonances of the urea's NH protons progressively collapse with the background of the spectra throughout the course of the titrations. All remaining resonances show upfield shifts. Furthermore, the macrocyclic resonances H-13 and H-16, together with those from the

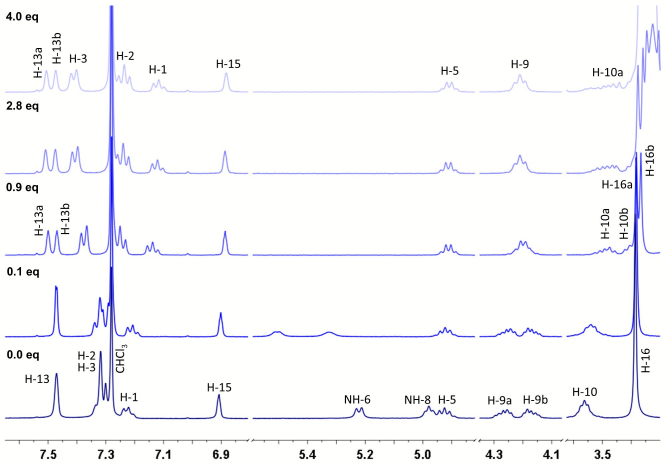

Figure 3. Relevant sections of ^{1}H NMR spectra in $CDCl_3$ of free **1** and upon addition of 0.1, 0.9, 2.8 and 4.0 equivalents of glu^{2-}.

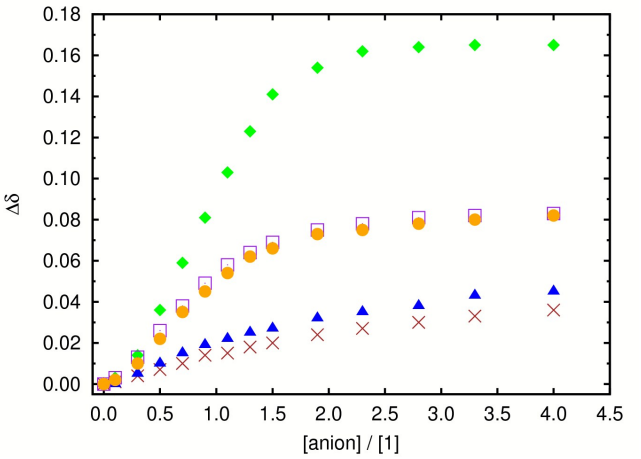

Figure 4. Chemical shift variation of H-3 from **1** along the titrations with aliphatic dicarboxylate anions ox^{2-} ( ), mal^{2-} (×), suc^{2-} (▲), glu^{2-} (□) and dg^{2-} (●).

spacers CH_2-10, tend to evolve into two distinct signals upon continuous addition of anion, while the two multiplets from CH_2-9 spacers collapse into one signal, typically a triplet.

These data suggest that the recognition of this subseries of anions (mal^{2-}, suc^{2-}, glu^{2-} and dg^{2-}) occurs with the urea pendant arms adopting a spatial disposition consistent with a conformation c_2, as further revealed by the preliminary docking studies carried out in gas phase (*vide infra*) and the molecular dynamics simulations in $CHCl_3$, illustrated in Figures 6 and S40.

In the case of the ox^{2-} interaction, the evolution of the signals from H-1, H-2, H-5, H-5', H-9a, H-9b, H-10a, H-10b and H-13 protons of **1** lead to a concavity in the titration curve before reaching the plateau, as depicted in Figure 5 for some of these signals. This behaviour suggests that the urea binding units are at least partially deprotonated promoting a through-bond electronic delocalization. Further insights into this particular feature would require the determination of the pK_a values for both carboxylate groups of ox^{2-}, which is hampered by the

insolubility of oxalic acid in chloroform. However, the evolution of H-3 aromatic resonances along the titration suggests the recognition of ox^{2-}; thus this behaviour is most probably owed to a consequent conformational change of **1**'s arms given the anion's small dimensions.

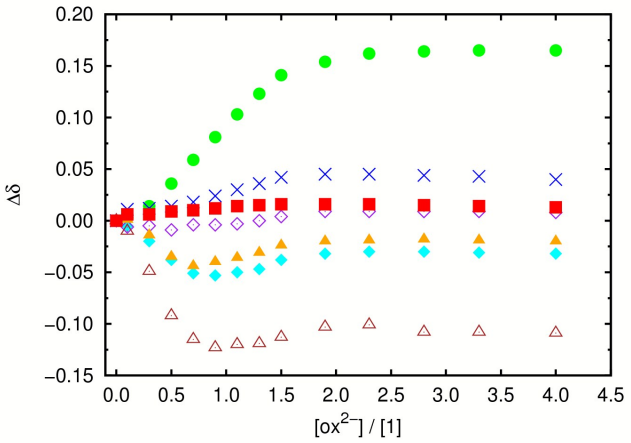

Figure 5. Chemical shift variation of H-3 (●), H-5 (×), H-9a ( ), H-9b (◊), H-10a (▲), H-10b (△) and H-13 (■) signals with the addition of ox^{2-} in $CDCl_3$.

All complexes exhibit a 1:1 stoichiometry by the Job plot method[29] using the H-3 data (see Figures S31-S35). Table 2 gathers the association constants (K_{ass}) between **1** and ox^{2-}, mal^{2-}, suc^{2-}, glu^{2-} and dg^{2-} anions. The constants were calculated with the HypNMR 2008 program[30] using the proton resonances with up- and downfield variations ($\Delta\delta = \delta_{obs} - \delta_{free}$) of $|\Delta\delta| > 0.025$ ppm and titration profiles typical of anion association, which are listed in Table S3.

Table 2. Values of K_{ass} /M^{-1} for the associations for ox^{2-}, mal^{2-}, suc^{2-}, glu^{2-} and dg^{2-} in $CDCl_3$.[a]

Anions	ox^{2-}	mal^{2-}	suc^{2-}	glu^{2-}	dg^{2-}
K_{ass} (M^{-1})	1694	286	983	2898	3104

[a] errors < 15%

The affinity of **1** for mal^{2-}, suc^{2-} and glu^{2-} anions significantly increases with the number of methylene groups between the two carboxylates. Indeed, the associations with glu^{2-} and the analogous dg^{2-} (this anion contains an ether oxygen at the central position of carboxylates linkage instead of a CH_2 group) display the highest constants of 2898 and 3104 M^{-1}, respectively. These results seem to indicate that the recognition of the two longest dicarboxylate anions occurs simultaneously by the two urea binding units, while the smaller ones (ox^{2-}, mal^{2-} and suc^{2-}) can be recognised intermittently by one or concomitantly by both urea binding units. On the other hand, the high association constant of 1694 M^{-1} observed for ox^{2-} eventually reflects the most negative electrostatic potential on the carboxylate groups of this anion relatively to the remaining dicarboxylate substrates, which may promote the conformational change of the two pendant arms necessary for the recognition of this smallest guest. Moreover, in contrast with mal^{2-}, suc^{2-}, glu^{2-} and dg^{2-} associations, **1** adopts a type c_1 conformation in the lowest energy structure of the association with ox^{2-}, as illustrated in Figure 6 (left) with a snapshot taken from the molecular dynamics simulation of this anion association.

Isomeric dicarboxylate anions. The enantioselective binding ability of **1** was evaluated towards the (*S,S*)- and (*R,R*)-$tart^{2-}$ enantiomers. The binding affinity for anionic geometric isomers of but-2-enedioic acid, fumarate (fum^{2-}) and maleate ($male^{2-}$) was also investigated. Selected ^{1}H NMR spectra from these titrations are presented in Figures S29-S30, with the corresponding proton resonances listed in Table S4.

The data obtained by ^{1}H NMR titrations show that the studied anions are recognized in a similar fashion as the aliphatic ones. Only one set of signals were found throughout the titration experiments, which is consistent with the recognition of the anions primarily by cooperative N-H···O hydrogen bonds between the NH protons and the carboxylate groups. In all cases the recognition of these anions is accompanied by a loss of symmetry in the macrocyclic platform, as revealed by the variations of H-13 resonance, as well as a conformational change of the two pendant arms. All associations showed a 1:1 stoichiometry as determined by Job plots (see Figures S36-S39). The corresponding calculated K_{ass} values are gathered in Table 3.

Table 3. K_{ass} (M^{-1}) values for the associations between **1** and the studied isomeric anions in $CDCl_3$.[a]

Anions	(*S,S*) $tart^{2-}$	(*R,R*) $tart^{2-}$	fum^{2-}	$male^{2-}$
K_{ass} (M^{-1})	2252	2090	4007	481

[a] errors < 15%.

Receptor **1** shows high affinity for both enantiomers of $tart^{2-}$ with the corresponding K_{ass} values indicating a slight preference for the (*S,S*)-$tart^{2-}$, but not enough to eventually promote their enantioselective discrimination. On the other hand, **1** is able to discriminate the geometric isomers fum^{2-} and $male^{2-}$ with association constants of 4007 and 481 M^{-1}, respectively. The signals of N-H urea binding units collapsed with the baseline in the presence of $male^{2-}$, which occurs upon addition of 2.3 equivalents of substrate. This finding suggests that an exchange between these protons and the oxygen atoms of the carboxylate groups from this anion can occur. In addition, the singlet resonances of H-13 and H-16 protons split in the presence of both anions, being this structural effect more pronounced with fum^{2-}.

Molecular modelling studies

Classical force field simulations. Aiming towards a comprehensive understanding of the dicarboxylate anions' recognition process at the molecular level, a molecular mechanics (MM) and Molecular dynamics (MD) study was carried out for the associations between **1** and the linear anions ox^{2-}, mal^{2-}, suc^{2-}, glu^{2-} and dg^{2-}, as well as for the geometric

isomers fum^{2-} and $male^{2-}$. This theoretical investigation was performed in $CHCl_3$[31] with Amber12,[32] using the General Amber Force Field (GAFF)[33] for the anions and receptor. The binding scenarios of each host-guest complex were obtained from a previous quenched MD run performed in gas-phase at 1000 K. Subsequently, a representative and low energy structure was selected, immersed in $CHCl_3$ periodic boxes and then subjected to at least three independent MD simulations, each with production runs of 50 ns. These MD replicates were preceded by force field parameterisation on the macrocycle, which is detailed below together with the complete MD simulation protocols.

The distance between the two urea binding units of **1** ($N_{urea}\cdots N_{urea}$) was calculated for the three independent production runs carried out for the seven anion associations, alongside the distance between the anion's carboxylate groups ($^{-}O_2C\cdots CO_2^{-}$). The wide range of $N_{urea}\cdots N_{urea}$ distances found for the seven host-anion systems, listed in Table S5, shows that the pendant arms experience significant conformational changes during the MD simulations, which are in agreement with the symmetry loss of **1** upon anion addition observed by ^{1}H NMR (*vide supra*). On the other hand, the average $N_{urea}\cdots N_{urea}$ distances calculated for the three independent MD runs for each ox^{2-}, mal^{2-}, suc^{2-}, glu^{2-}, dg^{2-} and fum^{2-} association are comparable, mirroring an equivalent anion binding behaviour throughout these replicates *(vide infra)*. In the case of the $male^{2-}$ association, the $N_{urea}\cdots N_{urea}$ distances in the initial three replicates showed an inconsistent behaviour, so four extra replicates were performed, totalling 350 ns of sampling data, which are carefully analysed below. Henceforth, the subsequent discussion of host-guest associations of aliphatic linear anions plus fum^{2-} will be based on structural data calculated using the concatenated trajectories of the three production runs; thus unless otherwise stated, a total sampling of 150 ns was used.

In all MD simulations undertaken with ox^{2-}, mal^{2-}, suc^{2-}, glu^{2-} and dg^{2-}, the most frequently observed binding scenario shows the anion positioned above the tetraazacalix[2]arene[2]triazine upper rim, between the two pendant arms, with each carboxylate group establishing intermittent N-H···O hydrogen bonds. This binding arrangement is labelled type A and is illustrated in Figure 6 with two selected snapshots taken from the MD simulations of ox^{2-} (left) and glu^{2-} (right) associations.

The N-H···O hydrogen bonds were assessed using cut-offs of 3.0 Å and 135° for N···O distances and N-H···O angles, respectively. Typically 2 or 3 hydrogen bonds were found, but for ox^{2-}, mal^{2-}, suc^{2-}, glu^{2-} and dg^{2-} associations, up to 6 were occasionally observed meaning that either the carboxylate oxygen atoms or the urea binding sites are involved in simultaneous hydrogen bonding interactions.

Subsequently, the occupancies of the established hydrogen bonds between the two oxygen atoms of each carboxylate binding site and both N-H groups of each urea binding moiety were summed and are plotted in Figure 7 for ox^{2-}, mal^{2-}, suc^{2-}, glu^{2-} and dg^{2-} associations with the cyan and red bars corresponding to the first and second urea binding units, respectively. The smaller anions, ox^{2-} and mal^{2-}, assume different binding poses during the MD production runs with the carboxylate groups swapping between the two urea binding moieties, so two sets of bars with different colours are depicted, one for each carboxylate group (*1* or *2*). Further insights into the anion recognition mechanism were obtained with the 3-D histograms created with the positions occupied by the oxygen atoms of each anion's carboxylate group throughout the individual MD runs. Indeed, the two 3-D histograms shown in Figure 8 for a single replicate of ox^{2-} and mal^{2-} associations are overlapped and rather diffuse, and show that both anions undergo a half-rotation, passing by intermediate binding scenarios where at least one carboxylate unit is hydrogen bonded to both urea binding arms. Furthermore, this binding scenario, termed as type B, exhibits different number of hydrogen bonds depending on the spatial disposition of the anion towards the receptor urea binding units. This behaviour is also illustrated in Figure 6 (middle) with a selected snapshot taken from the first replicate of the smallest anion association. Equivalent binding events were monitored for the remaining MD runs of **1**·ox^{2-} and **1**·mal^{2-}.

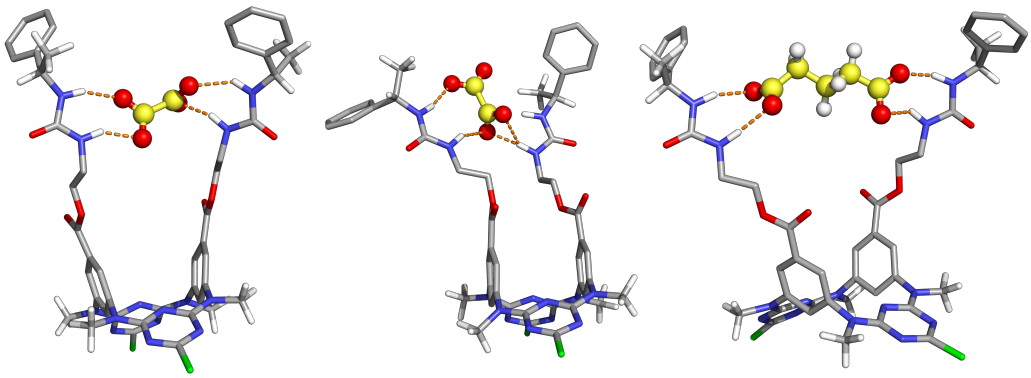

Figure 6. Selected snapshots taken from **1**·ox^{2-} and **1**·glu^{2-} MD simulations showing the type A (left and right) and B binding arrangements (middle). Hydrogen bonds are drawn as orange dashed lines. The carboxylate carbon and oxygen atoms are show in yellow and red spheres, respectively, while the remaining details are given in Fig. 1.

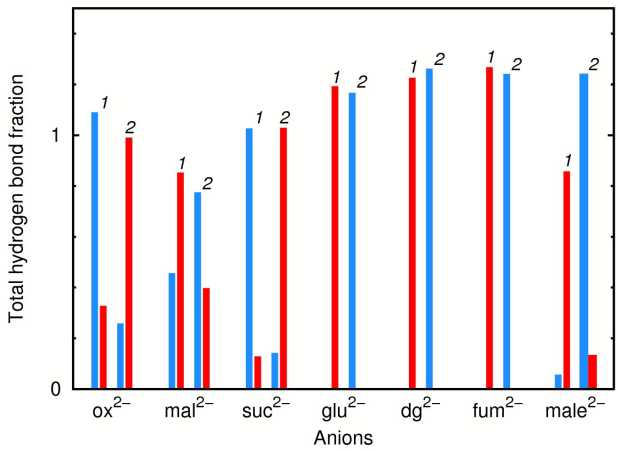

Figure 7. Bars graph showing the occupancies of the N-H···O hydrogen bonds between the carboxylate groups *1* and *2* of ox^{2-}, mal^{2-}, suc^{2-}, glu^{2-}, dg^{2-}, fum^{2-} and $male^{2-}$ anions and the urea binding units of **1** (blue and red).

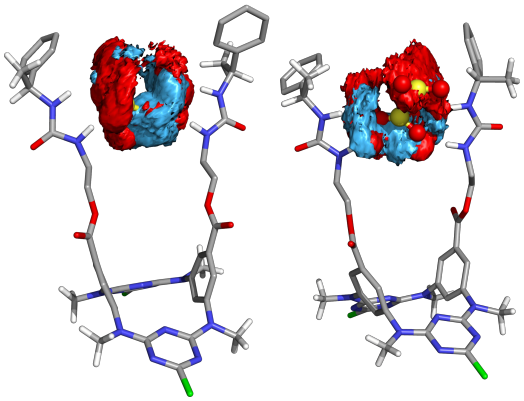

Figure 8. 3-D histograms built with the positions occupied by ox^{2-} (left) or mal^{2-} (right) carboxylate units one of the 50 ns of a MD simulation replicate. Each carboxylate unit (shown either in red or blue) is represented by the positions occupied by its oxygen atoms, 5 or more times. Remaining details as given in Fig. 6.

In contrast with the MD findings for **1**·ox^{2-} and **1**·mal^{2-} associations, the recognition of the larger anions glu^{2-} and dg^{2-} occurs exclusively through the type A binding scenarios, yielding two distinct and well-defined grid surfaces as illustrated in Figure 9, for a MD replicate of **1**·glu^{2-}. In agreement, only a set of blue and red bars is presented in Figure 7 for these two anion associations.

The suc^{2-} anion, with an intermediate size in the aliphatic linear anion series (see Scheme 1), seems to have a "transitional" binding behaviour between the observed for the smaller and larger anions. Indeed, in two replicates, each carboxylate group remains hydrogen bonded to a single urea binding entity throughout the 50 ns (as observed for glu^{2-} and dg^{2-}), while in the remaining one, a fast exchange of the carboxylate groups between the two urea binding units (binding scenarios of type A), preceded by a few records of type B binding scenarios. The 3-D histogram of this MD run, together with two binding scenarios of type A and B, are shown in Figure S40.

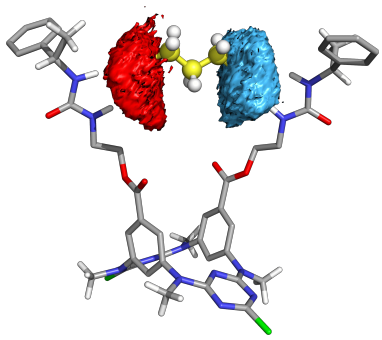

Figure 9. 3-D histograms built with the positions occupied by the glu^{2-} carboxylate units along one of the 50 ns of MD simulations. Each carboxylate unit (shown either in red or blue) is represented by the positions occupied by its oxygen atoms, 5 or more times.

Noteworthy, the **1**·fum^{2-} complex, with the anion's average $^{-}O_2C\cdots CO_2^{-}$ distances similar to suc^{2-} (see Table S6), exhibits a dynamic behaviour comparable to the complexes with the longer linear anions glu^{2-} and dg^{2-}. Therefore, in all replicates, the recognition of fum^{2-} occurs *via* a type A binding scenario, similarly to the one represented in Figure 9 for glu^{2-}.

As aforementioned, the MD runs carried out with $male^{2-}$ revealed that its recognition occurs through a complex process, which can involve extra binding arrangements than the ones reported for its geometric isomer fum^{2-}. While in the first replicate the anion is hydrogen bonded to **1** in a type A fashion, occasionally interrupted by a type B one, in the second replicate two new binding scenarios were observed, B' and C. In the type B' arrangement a single carboxylate group is exclusively shared by both urea binding moieties whilst the second carboxylate group is free of any interaction with the receptor, contrarily to type B. In the binding arrangement C, the anion binding occurs through one or two hydrogen bonds between a single carboxylate group and one urea binding unit. The B' and C type scenarios are depicted in Figure 10, together with the surface generated with the positions occupied by the oxygen atoms of the two-carboxylate groups for 50 ns of the second replicate. On the other hand, in the third replicate the binding type A is most frequently found followed by B'. It is worth mentioning that these odd scenarios are characterised by shorter average $N_{urea}\cdots N_{urea}$ distances, as shown in Table S5.

Given this different dynamical behaviour, the sampling of the $male^{2-}$ association was extended for four more replicates of 50 ns each. Three of them corroborate the first one, while the fourth is in agreement with the second replicate. In summary, these simulations show that the *cis* binding geometry of $male^{2-}$ determines its recognition mode, with arrangement C mostly maintained along 100 ns of MD sampling, which supports the lower constant experimentally observed for **1**·$male^{2-}$ (see Table 3).

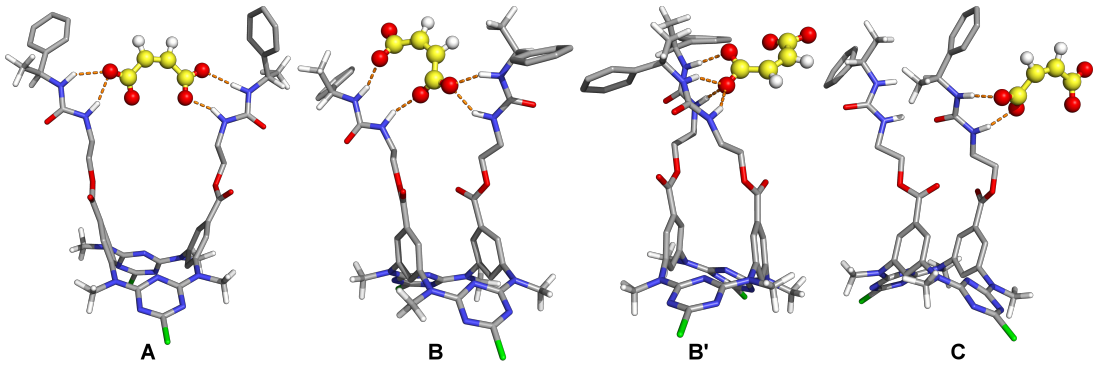

Figure 10. Binding scenarios A, B, B′ and C found throughout the initial MD simulations of **1**·male^{2-}. Remaining details as given in Fig. 6.

Table 4 lists the summation of the occupancies of the N-H···O hydrogen bonds established by the two indistinct NH-6 and NH-8 (see Scheme 1) binding units with the four carboxylate oxygen atoms. In all anion complexes, the two urea NH-8 binding sites systematically form a higher number of the hydrogen bonding interactions than the NH-6 ones. This *in silico* result supports the experimental NMR titration data and suggests that the access to both NH-6 binding sites is eventually limited by the steric bulk of the (*S*)-(*α*)-methylbenzyl adjacent substituent. In addition, the lower binding affinity of the NH-6 binding sites may also be dictated by their lower acidity comparatively with the NH-8 ones. Further insights were obtained through DFT calculations, as discussed below.

Table 4. Summation of occupancies of the N-H···O hydrogen bonds established by the two indistinct NH-6 and NH-8 sites of **1** with the anion carboxylate sites.

Anion	NH-6	NH-8
ox^{2-}	1.05	1.62
mal^{2-}	1.02	1.46
suc^{2-}	0.91	1.41
glu^{2-}	0.88	1.48
dg^{2-}	0.92	1.57
fum^{2-}	0.86	1.63
male^{2-}	1.01	1.28

The aforementioned MD results hint that the match between anion size, given by the average $^{-}O_2C\cdots CO_2^{-}$ distances collected in Table S6, and the $N_{urea}\cdots N_{urea}$ average distances (*vide supra*), play an important role on the binding affinity of **1** for the dicarboxylate anions. In this context, further relations between these structural parameters and the experimental association constants (Tables 2 and 3) were investigated. The plot of the average $N_{urea}\cdots N_{urea}$ distances computed for the mal^{2-}, suc^{2-}, glu^{2-} and dg^{2-} associations *versus* the $^{-}O_2C\cdots CO_2^{-}$ distances show a linear increase (see Figure 11) with a straight-line data fitting with R^2 = 0.96. Furthermore, both the $N_{urea}\cdots N_{urea}$ and $^{-}O_2C\cdots CO_2^{-}$ distances clearly reflect the K_{ass} values of these anions as depicted in Figure 12. Given the flexibility of the receptor urea binding moieties it is expected that the fit between the $N_{urea}\cdots N_{urea}$ distances and K_{ass} should be slightly smaller (R^2 = 0.93) than when the association constant values are plotted against the $^{-}O_2C\cdots CO_2^{-}$ distances (R^2 = 1.00). These remarkable linear fittings undoubtedly show that the affinity of **1** for linear aliphatic anions is dictated by the fine-tuning between the two binding units from the receptor and the separation between the two-carboxylate groups. The non-inclusion of ox^{2-} in this analysis is owed to the distribution of its electrostatic potential, as discussed below.

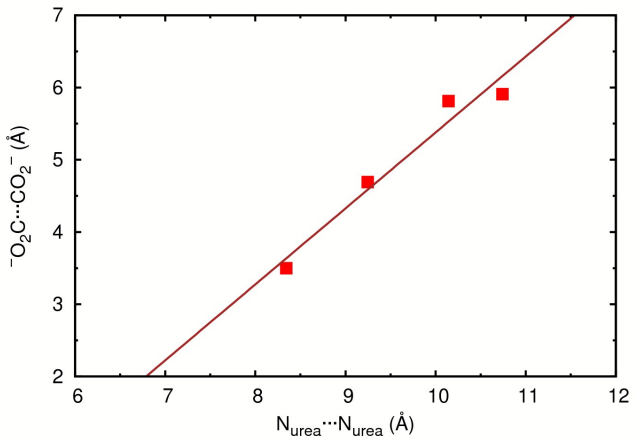

Figure 11. Plot of $^{-}O_2C\cdots CO_2^{-}$ distance (Å) as function of $N_{urea}\cdots N_{urea}$ distance (Å), showing a linear fitting.

In summary, our MD study led to an understanding, at the atomistic level, of how **1** recognizes a series of seven dicarboxylates composed of linear aliphatic anions with different chain size lengths (ox^{2-}, mal^{2-}, suc^{2-}, glu^{2-} and dg^{2-}) and two geometric isomers (fum^{2-} and male^{2-}). The detailed analysis of the MD structural data for the aliphatic anion complexes, apart from ox^{2-}, is consistent with the experimental affinity of **1** towards these anions.

All aforementioned simulations were carried out under charge neutrality conditions by the addition of two TBA counter ions in agreement with dicarboxylate salts used in the ^{1}H NMR titrations. Both counter-ions, initially positioned far away from each anion complex, were found in the vicinity of the receptor binding region surrounding the anion, after the equilibration

period of all MD replicates, as illustrated in Figure S41 for the suc^{2-} complex. The electrostatic attraction between the two TBA cations and the associated anions was aided by the hydrophobic nature of $CHCl_3$. In order to evaluate the contribution of the counter-ions on the stabilization of the different anion complexes, the MD simulations were repeated in more dilute conditions. In the first simulations, albeit the counter-ions were even further away, the TBA cations' approximation to each anion complex was observed again along with equivalent binding scenarios. Indeed, the average distances between the TBA and anion (centre of mass) for both setups range between 4.09 and 5.47 Å for the reported MD simulations and from 4.18 to 5.31 Å for the more diluted ones. However, to obtain further insights into this matter, the dynamical behaviour of the anion complexes was also investigated in the absence of TBA counter-ions using the net charge neutralizing plasma. In these simulation conditions, equivalent binding scenarios were also observed, but with a more frequently interchange rate, which suggests that the counter-ions may contribute to the stabilization of the anion complexes.

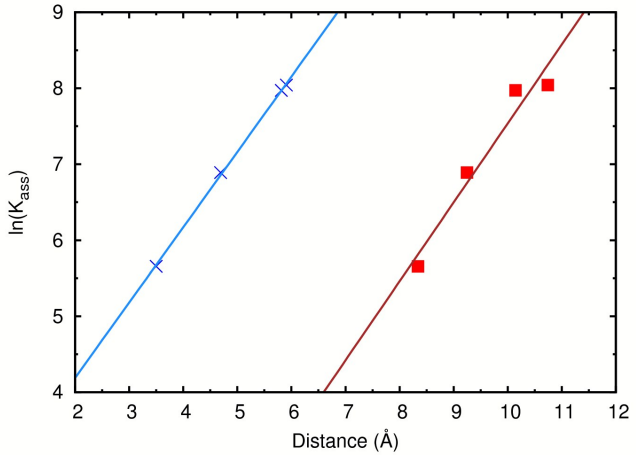

Figure 12. Representation of $\ln(K_{ass})$ as function of $^{-}O_2C\cdots CO_2^{-}$ distances (Å, ×) or $N_{urea}\cdots N_{urea}$ distances (Å, ■), showing linear fittings.

The quantitative analysis of the high affinity of **1** for the different anions could be accomplished by the computation of the binding free energies, including the enthalpy and entropy components, which could be straightforwardly assessed from unrestrained MD simulation data through the MM-PBSA approach. Unfortunately, to the best of our knowledge, this method is only parameterised for water and not for chloroform. Furthermore, the use of more sophisticated free energy calculations based on MD simulations is beyond the scope of this work.

Electrostatic potential calculations. The electrostatic potential computed on a molecule's electron density surface (V_S) has been widely employed to evaluate non-covalent interactions containing a significant electrostatic component.[34] Moreover, the most positive values ($V_{S,max}$) are clearly related with hydrogen-bond acidity[35] and consequently with the receptor's anion binding ability;[36] on the other hand, the most negative values ($V_{S,min}$) can be used to rationalise the anion hydrogen-bond basicity.[37] In order to bring further insights into the interaction strength between **1** and the carboxylate anions' series, the electrostatic potentials of the free macrocycle and the anionic species were calculated with Gaussian 09[38] using the B3PW91 hybrid functional combined with the 6-311+(d,p) basis set for the anions or with the 6-311(d,p) basis set for **1**. The remaining computational details are given below.

The relevant V_S values, including $V_{S,max}$ and $V_{S,min}$, are listed in Table 5 for the seven carboxylate anions, while Figure 13 depicts the distribution of the electrostatic potential mapped onto the electron density surface of ox^{2-} and glu^{2-} with selected Vs values located near the carboxylate bindings highlighted with green dots ($V_{S,carb}$) and $V_{S,min}$ values as a blue dots. Overall, the less negative region of the electrostatic potential (red surface) was found for all anions over the space between the two carboxylate groups, apart from ox^{2-}, in which each oxygen atom is enclosed by a red area.

Table 5. Electrostatic potential values (kcal mol^{-1}) at selected points on the molecular surface of the carboxylate anions. When appropriate, the average value of the homologous/symmetric points is given.

Anion	$V_{S,min}$	$V_{S,carb}$	$V_{S,max}$
ox^{2-}	-231.33	-225.74	-207.59
mal^{2-}	-242.77	-217.17	-158.51
suc^{2-}	-207.67	-207.67	-154.19
glu^{2-}	-200.45	-200.45	-135.14
dg^{2-}	-222.42	-199.37	-135.32
$male^{2-}$	-206.66	-206.66	-160.30
fum^{2-}	-229.78	-213.28	-132.89

The negative electrostatic potential of ox^{2-} ranges between -231.33 and -207.59 kcal mol^{-1}, being spread throughout the very small anion surface with four distinct Vs$_{,min}$ positioned between the carboxylate groups and symmetrically distributed relatively to the C-C central bond (see Figure 13), while the $V_{S,carb}$ has an energy of -225.74 kcal mol^{-1}. These points are naturally relevant for the simultaneous recognition of each carboxylate by a urea binding moiety and are also shown in Figure 13 as green dots. This electrostatic potential distribution is consistent with relative high affinity of **1** for ox^{2-} as well as with partial deprotonation of the receptor observed in the titration experiments. The mal^{2-} anion exhibits a single Vs$_{,min}$ of -242.77 kcal mol^{-1} (see Figure S42), located between the two carboxylate groups, followed by two $V_{S,carb}$ with energy of -217.17 kcal mol^{-1}, which are less negative than the $V_{S,carb}$ for ox^{2-}, coming in agreement with a superior affinity of **1** for the smaller anion. On the other hand, suc^{2-} and glu^{2-} have two $V_{S,min}$ with average energies of -207.67 and -200.45 kcal mol^{-1} respectively, which also correspond to $V_{S,carb}$ as depicted in Figures S42 and 13, respectively. The distribution of the electrostatic potential of the dg^{2-} anion, in Figure S42, shows two $V_{S,min}$ equidistant of the ether oxygen atom with an energy of -222.42 kcal mol^{-1} and two $V_{S,carb}$ of 199.37 kcal mol^{-1}. In other words, along the aliphatic anion series, from mal^{2-} to

glu^{2-}, the $V_{S,carb}$ becomes less negative as the anion size increases, and a linear trend (R^2 = 1.00) can be found between the $V_{S,carb}$ values and the association constants, as depicted in Figure 14. Therefore, this comparison suggests that along this series the strength of the receptor-anion interaction is not dictated by this quantum descriptor, but by other effects (*vide supra*) including the match between the anion chain length and the separation between the two urea binding units, which becomes progressively the preferential recognition mechanism going from mal^{2-} to dg^{2-} as shown by molecular dynamics simulations.

Likewise glu^{2-} and suc^{2-}, the linear fum^{2-} anion presents two well-defined $V_{S,min}$ dots, coincident with $V_{S,carb}$, of -206.66 kcal mol^{-1} while its geometric isomer $male^{2-}$ exhibits two $V_{S,min}$ of -229.78 kcal mol^{-1} between two carboxylate groups and two $V_{S,carb}$ of -213.28 kcal mol^{-1} (see Figure S42). Again this comparison shows that the superior affinity of **1** for fum^{2-} cannot be found through the electrostatic potential distribution.

The analysis of the distribution of the electrostatic potential on the molecular surface of **1**, given in Figure 13, clearly shows that the most acidic regions correspond to the urea binding units. However, it is worth mentioning that for each urea moiety, the $V_{S,max}$ (52.53 and 51.40 kcal mol^{-1} for each binding site) can be found closer to NH-8 than to NH-6, thus corroborating the referred NMR data interpretation. In other words, the superior binding affinity of NH-8 urea sites seems to be determined by their slightly higher acidity comparatively with NH-6, eventually assisted by the steric hindrance caused by the (*S*)-(*α*)-methylbenzyl substituents attached to the NH-6 binding sites.

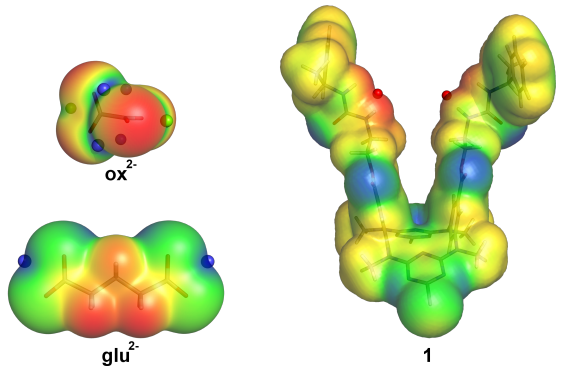

Figure 13. Electrostatic potential mapped on the molecular electron density surface (0.001 electrons per $Bohr^3$) of ox^{2-}, glu^{2-} and **1**. The $V_{S,min}$, $V_{S,carb}$ and $V_{S,max}$ are respectively represented by blue, green and red dots on the molecular surfaces. The colour scales range from blue to red as follows: ox^{2-} [-231.4; -207.6 kcal mol^{-1}]; glu^{2-} [-200.5 ; -135.1 kcal mol^{-1}]; and **1** [-36.9 ; 52.5 kcal mol^{-1}].

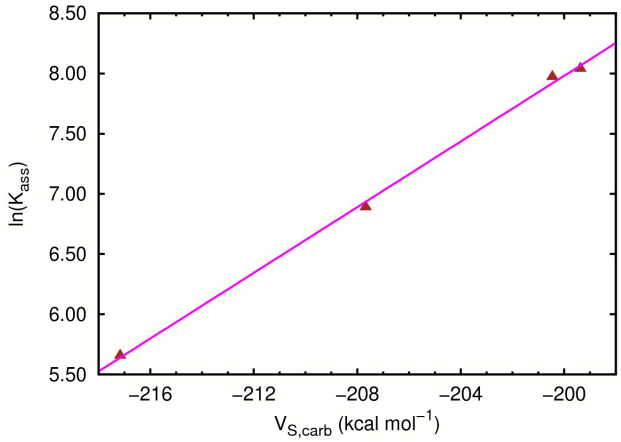

Figure 14. Representation of $\ln(K_{ass})$ as function of $V_{S,carb}$, showing a linear fitting.

Conclusions

A new anion receptor based on the dichloroazacalix[2]arene[2]triazine platform was prepared in good yield following a stepwise synthetic pathway, in which the urea binding entities were appended to *m*-phenylenediamine moieties before the macrocyclization process. The ^{1}H NMR titrations in $CDCl_3$ showed that both flexible arms of **1** are able to cooperatively recognise the studied dicarboxylate anions. Moreover, the MD simulations show that the receptor binds the anionic substrates through intermittent N-H···O hydrogen bonds using four possible binding scenarios of type A, B, B' and C, depending on the anion's size and binding geometry. Noteworthy, the larger anions glu^{2-} and dg^{2-}, with higher K_{ass} values (2898 and 3104 M^{-1}, respectively), exclusively adopt a type A binding arrangement, which is characterised by the interaction of both carboxylates with the two urea binding units. On the other hand, the smaller anions ox^{2-} and mal^{2-} oscillate within the receptor binding region, between binding scenarios A and B, eventually passing through type B'. In addition, the K_{ass} values for mal^{2-}, suc^{2-}, glu^{2-}, dg^{2-} anions follow a straight-line fitting with the average distances between the carboxylate groups, as well as between the urea binding moieties of **1**, as calculated from MD simulations, which suggests that the receptor binding affinity is determined by the fitting between anion size and the separation between the urea pendant arms.

In spite of the good affinity of **1** for both (*S,S*)- and (*R,R*)-$tart^{2-}$ anionic guests, the similar associations are inconsistent with enantioselectivity. On the other hand, **1** selectively binds the fum^{2-} and $male^{2-}$ geometric isomers with association constants of 4007 *vs* 481 M^{-1}, respectively. The recognition of fum^{2-} occurs mainly through the type A binding arrangement, while the A, B' and C scenarios contribute almost equally for the binding of $male^{2-}$, which may explain the lower association constant found for this anion.

The MD simulations on all anion complexes show that the carboxylate groups preferentially establish N-H···O hydrogen bonds with NH-8 urea binding units rather than NH-6, which is in agreement with $V_{S,max}$ values calculated for the receptor and with the ^{1}H NMR binding data.

Experimental Section

General remarks

All reagents were used as supplied without further purification. All organic solvents were purified and dried before use according to standard methods.[39] Uncorrected melting points were determined with a Reicher Model Thermovar melting-point apparatus. LRMS spectra were obtained on a Bruker Daltonic Esquire 3000 Ion Trap Mass Spectrometer with ESI-ITD-MS/MS negative ion mode while HRMS (ESI) experiments were performed on a Bruker Daltonics ApexQe FTICR Mass Spectrometer equipped with a combined Apollo II electrospray/MALDI ion source and a 7T actively shielded superconduting magnet. ^{1}H and ^{13}C APT spectra were recorded at 298 K on a Bruker Avance 400 spectrometer operating at 400.13 and 100.61 MHz, respectively, using DMSO-d_6 (99.9%) or $CDCl_3$. The 2D NMR (HMBC, HMQC, COSY) experiments were acquired using the same apparatus. The VT ^{1}H NMR experiments with **1** were carried out in $CDCl_3$ at 269, 257, 245 and 234 K. All chemical shifts are presented in ppm and using tetramethylsilane as internal reference.

(*S*)-1-(2-Hydroxyethyl)-3-(1-phenylethyl)urea, 3. Ethanolamine (0.428 mL, 7.10 mmol) was added to a solution of (*S*)-*α*-methylbenzyl isocyanate **2** (0.523 g, 3.55 mmol) in $CHCl_3$ (15 mL) at room temperature. After 19h the solution was concentrated forming a yellow solid which was recrystallized from ethyl acetate. Urea **3** (686 mg) was obtained as a white solid with 93% yield, m.p. = 147 °C. $[\alpha]_D^{20}$ +13.99 (c = 0.022; $CHCl_3$); IR (KBr): ν_{max} 3334 (NH), 3054, 3034 (C-H Ar), 2965, 2932 (CH aliphatic), 1628 (C=O urea), 1589, 1578, 1538 (C-N-H urea), 1493 (CC Ar), 1463, 1443 (CC aliphatic), 1262 (C-N), 1054, 1030 (C-O alcohol), 747, 699 (C-H Ar) cm^{-1}; ^{1}H NMR (400.13 MHz, $CDCl_3$) δ 7.08–7.00 (m, 5H, H-1, H-2, H-3), 5.73 (d, J = 7.0 Hz, 1H, NH-6), 5.51 (t, J = 5.4 Hz, 1H, NH-8), 4.79 (quint, J = 7.0 Hz, 1H, H-5), 3.55–3.49 (m, 2H, H-10), 3.23–3.10 (m, 2H, H-9), 1.39 (d, J = 7.0 Hz, 3H, H-5') ppm; ^{13}C NMR (100.61 MHz, $CDCl_3$) δ 159.1 (C-7), 144.4 (C-4), 128.6 (C-2), 127.1 (C-1), 125.8 (C-3), 62.7 (C-10), 49.9 (C-5), 42.9 (C-9), 23.2 (C-5') ppm; ESI-MS *m/z* 209 $[M+H]^+$.

(*S*)-2-(3-(1-phenylethyl)ureido)ethyl 3,5-dinitrobenzoate, 4. To a solution of **3** (450 mg, 2.16 mmol) in THF (13 mL) containing K_2CO_3 (894 mg, 6.48 mmol) , 3,5-dinitrobenzoyl chloride (498 mg, 2.16 mmol) in THF (5.6 mL) was slowly added. After 18h of stirring, the reaction mixture was decanted and evaporated. **4** (756 mg) was obtained after recrystallization from ethyl acetate with 87% yield, m.p. = 269 °C. $[\alpha]_D^{20}$ +101.70 (c = 0.020; $CHCl_3$); IR (KBr) ν_{max} 3355, 3299 (NH), 3100, 3080 (C-H Ar), 2966, 2927 (CH aliphatic), 1735 (C=O ester), 1628 (C=O urea), 1570, 1547 (C-N-H urea), 1493 (CC Ar), 1451 (CC aliphatic), 1346 (NO_2), 1279 (C-N), 1076 (C-O ester), 731, 721 (C-H Ar) cm^{-1}; ^{1}H NMR (400.13 MHz, $CDCl_3$) δ 9.21 (t, J = 1.8 Hz, 1H, H-15), 9.09 (d, J = 1.8 Hz, 2H, H-13), 7.34–7.20 (m, 4H, H-2, H-3), 7.14 (t, J = 6.5 Hz, 1H, H-1), 5.04 (d, J = 6.1 Hz, 1H, NH-6), 4.91 (sl, 1H, NH-8), 4.77 (quint, J = 6.7 Hz, 1H, H-5), 4.54–4.36 (m, 2H, H-10), 3.66–3.54 (m, 2H, H-9), 1.43 (d, J = 6.7 Hz, 3H, H-5') ppm; ^{13}C NMR (100.61 MHz, $CDCl_3$) δ 162.5 (C-11), 157.4 (C-7), 148.5 (C-14), 143.9 (C-4), 133.5 (C-12), 129.5 (C-13), 128.7 (C-2), 127.3 (C-1), 125.7 (C-3), 122.4 (C-15), 66.3 (C-10), 50.4 (C-5), 39.1 (C-9), 23.5 (C-5') ppm; ESI-MS *m/z* 403 $[M+H]^+$, 425 $[M+Na]^+$.

(*S*)-2-(3-(1-phenylethyl)ureido)ethyl 3,5-diaminobenzoate, 5.[24] Compound **4** (840 mg, 2.09 mmol) and Pd/C(en) 10% (m/m) (84 mg) in EtOH (40 mL) were mechanically stirred in a parr reactor under H_2 atmosphere at ≈50 psi during 2h. The mixture was poured through a celite filter and the solvent evaporated at reduced pressure, quantitatively yielding **5** (713 mg) as a white foam. ^{1}H NMR (400.13 MHz, $CDCl_3$) δ 7.33–7.24 (m, 4H, H-2, H-3), 7.23–7.16 (m, 1H, H-1), 6.62 (d, J = 2.0 Hz, 2H, H-13), 6.15 (t, J = 2.0 Hz, 1H, H-15), 5.53 (d, J = 7.0 Hz, 1H, NH-6), 5.27 (t, J = 5.5 Hz, 1H, NH-8), 4.78 (quint, J = 7.0 Hz, 1H, H-5), 4.22–4.09 (m, 2H, H-10), 3.46–3.30 (m, 2H, H-9), 1.33 (d, J = 7.0 Hz, 3H, H-5') ppm.

(*S*)-2-(3-(1-phenylethyl)ureido)ethyl 3,5-bis((4.6-dichloro-1.3.5-triazin-2-yl)amine)benzoate, 6.[19] A mixture of **5** (702 mg, 2.05 mmol) and diisopropylethylamine (0.89 mL, 5.13 mmol) in THF (8 mL) was added drop wise to a solution of cyanuric chloride (751 mg, 4.10 mmol) in THF (22 mL) at -12 °C. After stirring for 2 h without controlling the temperature, the reaction mixture was filtered and concentrated, forming a yellow solid which was not completely purified by column chromatography and recrystallization. ^{1}H NMR (400.13 MHz, DMSO-d_6) δ 11.00 (s, 2H, NH-16), 8.04 (d, J = 1.9 Hz, 2H, H-13), 7.90 (t, J = 1.9 Hz, 1H, H-15), 7.31–7.22 (m, 4H, H-2, H-3), 7.20–7.13 (m, 1H, H-1), 4.72 (q, J = 7.0 Hz, 1H, H-5), 4.30–4.20 (m, 2H, H-10), 3.44–3.28 (m, 2H, H-9), 1.28 (d, J = 7.0 Hz, 3H, H-5') ppm.

$(NH)_4$-azacalix[2]arene[2]triazine, 7.[20-21, 23] Diamine **5** (211 mg, 0.33 mmol) and trimer **6** (113 mg, 0.33 mmol), each previously dissolved in acetone (28 mL), were simultaneously added drop wise at the same rate to a solution of diisopropylethylamine (0.144 mL, 0.83 mmol) in acetone (66 mL) at 65° C for 8 h. The reaction mixture was stirred under nitrogen at room temperature and a white solid began to precipitate. After 7 days, the reaction mixture was concentrated to 1/3 of the volume and then the solid was filtered off and washed with water and cold acetone. The $(NH)_4$-azacalix[2]arene[2]triazine **7** was obtained (153 mg, 51%.) as a white solid. m.p. > 350 °C. $[\alpha]_D^{20}$ +98.76 (c = 0.018; DMSO); IV (KBr): ν 3308 (NH), 3087, 3028 (C-H Ar), 2974 (CH aliphatic), 1719 (C=O ester), 1622 (C=O urea), 1557 (C-N-H urea), 1444 (CC aliphatic), 1227 (C-N), 1025 (C-O ester), 883, 801, 768, 701 (C-H Ar) cm^{-1}; ^{1}H NMR (400.13 MHz, DMSO-d_6) δ 10.19 (s, 4H, H-16), 7.97 (t, J = 1.8 Hz, 2H, H-15), 7.41 (d, J = 1.8 Hz, 4H, H-13), 7.26–7.18 (m, 8H, H-2, H-3), 7.14

(td, J = 6.9, 1.8 Hz, 2H, H-1), 6.40 (d, J = 7.3 Hz, 2H, NH-6), 5.95 (t, J = 5.7 Hz, 2H, NH-8), 4.68 (quint, J = 7.3 Hz, 2H, H-5), 4.24–4.16 (m, 4H, H-10), 3.41–3.27 (m, 4H, H-9), 1.24 (d, J = 7.3 Hz, 6H, H-5') ppm; ^{13}C NMR (100.61 MHz, DMSO-d_6) δ 168.3 (C-18), 164.7 (C-11), 164.6 (C-17), 157.2 (C-7), 145.7 (C-4), 138.3 (C-14), 130.6 (C-12), 128.2 (C-2), 126.4 (C-1), 125.7 (C-3), 123.9 (C-15), 119.9 (C-13), 64.7 (C-10), 48.6 (C-5), 38.3 (C-9), 23.3 (C-5'); HRMS (ESI) calcd. for $C_{42}H_{42}Cl_2N_{14}O_6^+$ $[M+H]^+$: 907.27051, found 907.26710.

(NMe)$_4$-azacalix[2]arene[2]triazine, 1. MeI (90 μL, 1.453 mmol) was added to a dispersion of **7** (314 mg, 0.346 mmol) and Cs_2CO_3 (1.803 g, 5.54 mmol) in acetonitrile (11 mL). After 20 h stirring at room temperature, an NH_4Cl saturated aqueous solution (5 mL) was added and stirred for an additional 15 minutes. The mixture was concentrated and the product extracted with dichloromethane. The unreacted **7** (159 mg) was filtered off and further reacted in the same conditions. After 4 consecutive reactions, the crude product was purified by column chromatography (cyclohexane/acetone 2:1), obtaining **1** (243 mg) as a white solid with 73% yield. Crystalline needles of **1** were grown by slow evaporation of a toluene/dichloromethane/methanol/water/ isopropanol solution, m.p. > 350 °C. $[\alpha]_D^{20}$ +122.62 (c = 0.018; $CHCl_3$); IR (KBr): ν_{max} 3366 (NH), 3076, 3030 (C-H Ar), 2970, 2930 (CH aliphatic), 1727 (C=O ester), 1637 (C=O urea), 1568 (C-N-H urea), 1492 (CC Ar), 1452, 1403 (CC aliphatic), 1235 (C-N), 1026 (C-O ester), 857, 802, 700 (C-H Ar) cm^{-1}; ^{1}H NMR (400.13 MHz, $CDCl_3$) δ 7.48–7.45 (m, 4H, H-13), 7.36–7.25 (m, 8H, H-2, H-3), 7.14 (td, J = 7.0, 1.7 Hz, 2H, H-1), 6.90 (t, J = 1.7 Hz, 2H, H-15), 5.25 (d, J = 6.8 Hz, 2H, NH-6), 4.99 (t, J = 4.9 Hz, 2H, NH-8), 4.92 (quint, J = 6.8 Hz, 2H, H-5), 4.31–4.22 (m, 2H, H-10a), 4.22–4.12 (m, 2H, H-10b), 3.60–3.52 (m, 4H, H-9), 3.38 (s, 12H, H-16), 1.46 (d, J = 6.8 Hz, 6H, H-5') ppm; ^{13}C NMR (100.61 MHz, $CDCl_3$) δ 169.9 (C-18), 165.6 (C-11), 165.3 (C-17), 157.7 (C-7), 145.6 (C-14), 144.0 (C-4), 132.0 (C-15), 131.7 (C-12), 128.7 (C-2), 128.0 (C-13), 127.3 (C-1), 125.9 (C-3), 65.2 (C-10), 50.0 (C-5), 39.1 (C-9), 37.4 (C-16), 23.1 (C-5') ppm; HRMS (ESI) *m/z* calcd. for $C_{46}H_{49}Cl_2N_{14}O_6^+$, 963.33311; found, 963.33013.

Tetrabutylammonium carboxylate salts. The carboxylate anions (ox^{2-}, mal^{2-}, suc^{2-}, glu^{2-}, dg^{2-}, (*R*,*R*)-$tart^{2-}$, (*S*,*S*)-$tart^{2-}$, fum^{2-}, $male^{2-}$) were used as tetrabutylammonium salts. They were prepared mixing 2 equivalents of a methanolic solution of tetrabutylammonium hydroxide (1.27 M) with a solution of carboxylic acid in methanol during 2 h in the absence of light. Subsequently, the solvent was evaporated and the salts were recrystallized from acetone/ethanol and dried under high vacuum overnight. The purity of the salts was confirmed by ^{1}H NMR spectroscopy.

NMR studies

The tetrabutylammonium anion salts used as substrates were prepared as described above. The ^{1}H NMR studies were carried out using two NMR tubes simultaneously, each of them loaded with 400 μL of receptor solution in $CDCl_3$ (c_i=4.0×10^{-3} M). After collecting the spectrum of the free receptor, aliquots of anionic solutions in $CDCl_3$ were added (0.1, 0.3, 0.5, 0.7, 0.9, 1.1, 1.3, 1.5, 1.9, 2.3, 2.8, 3.3 and 4.0 equivalents) using a Hamilton syringe (Microliter 1700 series, 10 μL) followed by vigorous mixing. After waiting 7-10 minutes to attain equilibrium, the spectrum was recorded and the addition of each aliquot of the anions was separated by approximately 15 minutes. These experiments were carried out in a Bruker Avance 400 at 298 K. No effort was made to maintain the ionic strength constant in order to avoid the competition of other anions. Each titration was done at least twice.

The association constants of the species formed in solution were determined by best fitting the precise value of the species' concentrations in solution and the observed ^{1}H chemical shifts using HypNMR 2008. The errors quoted in parenthesis are the standard deviations of the overall stability constants, which are calculated directly by HypNMR from the input data.

The stoichiometry of the associations was determined by means of Job plots. Solutions of the receptor and of the anions in $CDCl_3$ were prepared with concentrations of 4.0×10^{-3} M, which were subsequently mixed in different proportions (v/v) in NMR tubes: 500:0, 450:50, 400:100, 350:150, 300:200, 250:250, 200:300, 150:350, 100:400, 50:450 and 0:500.

X-ray crystallography

Single crystal X-ray diffraction data **1** were collected on a Bruker SMART APEX II diffractometer with a CCD area detector using graphite monochromatised Mo-Kα radiation (λ = 0.71073 Å) at 150(2) K. The frames were integrated with the SAINT-Plus software package,[40] and the intensities were corrected for polarization and Lorentz effects. Absorption correction was applied *via* multi-scan procedure using the SADABS42 from the same graphical suite. The structure was solved by a combination of direct methods with subsequent difference Fourier syntheses and refined by full matrix least squares on F^2 using the SHELX-2013 suite.[42] Anisotropic thermal displacements were used for all non-hydrogen atoms. The hydrogen atoms were inserted at geometrical positions with U_{iso} = 1.2U_{eq} to those that are attached. The crystal data and refinement details are summarized in Table S2. The ORTEP diagram shown in Figure 1 was drawn with OLEX2 software.[43] Crystal structure data has been deposited with the Cambridge Crystallographic Data Centre, CCDC: 1030650. Copy of the data can be obtained free of charge on application to CCDC, 12 Union Road, Cambridge CB2 1EZ, UK fax (+44) 1223 336033, e-mail: deposit@ccdc.cam.ac.uk.

Computational methods

All quantum calculations were carried out with Gaussian09,[38] while the MM calculations and MD simulations were undertaken with Amber12[32] using RESP charges[44] and parameters taken from the General Amber Force Field (GAFF).[33]

This computational study began with the optimisation of the four independent conformations of **1**, directly taken from the asymmetric unit of its crystal structure, at HF/6-31G(d), followed by a single point RESP charge calculation at the same

level of theory using the Gaussian IOp: 6/33=2, 6/41=4, 6/42=6 according to GAFF. RESP charge fitting of the concatenated ESP data of these structures afforded the final atomic point charges of **1** used in the subsequent MM calculations and MD simulations. The atomic charges used for carboxylate anions apart from ox^{2-}, as well as for tetrabutylammonium counter-ion (TBA), were estimated as follows. The initial structure of each ionic species was directly obtained from a suitable X-ray diffraction crystal structure deposited with CCDC[45] and subsequently their RESP charges were calculated as reported for the macrocycle.

To obtain partial atomic charges less dependent on the molecular conformation and orientation, each molecule underwent a gas-phase MD run at 1000 K for 10 ns, using a 1 fs time step, after a short heating period of 50 ps. Frames were saved every 1 ps given a trajectory file containing 10000 structures, which were further minimised by MM, energy sorted and clustered by root-mean-square deviation (RMSD). Low energy conformations from different clusters, three for the anions and five for TBA, were selected for subsequent HF/6-31G(d) geometry optimizations followed by ESP calculations. ESP data obtained for these conformations together with the ESP data previously calculated for the initially optimized structures were concatenated and then improved atomic point charges for each of this ionic species were obtained through RESP fitting using identical weights for all conformations. The RESP atomic charges of ox^{2-}, fum^{2-} and $male^{2-}$ were obtained from a single conformation.

The MM calculations and MD simulations on host-guest associations **1**·**A**, (A = ox^{2-}, mal^{2-}, suc^{2-}, glu^{2-}, dg^{2-}, fum^{2-} and $male^{2-}$) were preceded by the force field parameterisation on the azacalix[2]arene[2]triazine platform. In a previous publication,[20] we have reported that the default GAFF parameters are not suitable to accurately describe the structural features of this macrocyclic skeleton due to the intermediate sp^2/sp^3 character of the nitrogen bridging atoms. Specific parameters for bond and angle terms involving these atoms were then developed using single crystal X-ray diffraction data from azacalix[2]arene[2]triazine derivatives. In this work, these parameters were recalculated using a larger data series composed of sixteen single crystal X-ray diffraction structures; sixteen deposited with CCDC[45] and two unpublished ones from our laboratory. Three new atom types were created, as depicted in Figure S43, NH for nitrogen bridging atoms and CT and CX for the triazine and phenyl carbon atoms, respectively, and directly bonded to nitrogen bridging atoms. The remaining atoms were assigned with GAFF default atom types. The NH−CX and NH−CT equilibrium bond lengths and CX−NH−CT equilibrium bond angles used were the average values calculated with this structural data series and the corresponding force constants were calculated using the appropriate GAFF equations.[33] The force constants for all angles involving these new atom types and the default ones were recalculated considering the new NH−CX and NH−CT ideal distances. The dihedral angles subtended at the C−N bridges were also changed accordingly to Table S7, which lists all force field adjustments. This new parameter set was validated by the comparison of the RMSD values between the gas-phase MM structures optimised with GAFF default parameters and with new parameter data set against the corresponding crystal structure. Overall, the RMSD values listed in Table S8 show that a much better fitting is obtained with modified parameters, apart from molecules **1** and **L2**. In the crystal structures of both compounds a network of intermolecular hydrogen bonds is observed, which are obviously not accounted in the gas-phase optimizations.

Afterwards, the host-guest complexes **1**·**A** were generated by positioning the anion on the upper rim of **1** between the urea binding sites. Each anion complex was then submitted to a stochastic conformational analysis following the quenched molecular dynamics procedure described above.

A low energy and representative structure of each anion complex was selected and solvated with all-atom model of chloroform molecules[31] affording a cubic box. The charge neutrality was achieved by addition of two TBA counter-ions. Subsequently each system was equilibrated under periodic boundary conditions using the following multi-stage protocol. The solvent molecules were minimized by MM, keeping the solute fixed with a positional restraint of 500 kcal mol^{-1} $Å^{-2}$. Then, the restraint was removed and the entire system was allowed to relax. The system was subsequently heated to 300 K for 50 ps with a weak positional restraint (10 kcal mol^{-1} $Å^{-2}$) on the solute using the Langevin thermostat with a collision frequency of 1 ps^{-1} in an NVT ensemble. The positional restraint was then removed and the system was allowed to equilibrate in a NPT ensemble (300 K, 1 atm) for 2 ns. Finally, NPT data collection runs were performed over 50 ns and snapshots were saved to a trajectory every 1 ps. Two replicas for each system were undertaken using Amber 12 GPU accelerated code.[46] Bond lengths involving all bonds to hydrogen atoms were constrained with the SHAKE algorithm.[47] The Newton equations of motion were integrated with a 2 fs time step. The Particle Mesh Ewald method[48] was used to treat the long-range electrostatic interactions and the non-bonded van der Waals interactions were truncated with a 10 Å cut-off. The production data were analysed with cpptraj.[49]

The electrostatic potential calculations were carried out using as starting geometries structures previously optimised for the first atomic charge calculations, whereas for the anion complexes representative structures taken from MD simulations were used. These structures of the anions were optimised at B3PW91/6-311+G(d,p) and, afterwards, single point electrostatic potential energy calculations at the same theory level were performed in order to obtain the electrostatic potential (V_S) mapped onto the electron density surface of the individual anions or the anion complexes. The electrostatic potential of the macrocycle was obtained at B3PW91/6-311+G(d,p) using a structure previously optimised with the same hybrid functional and basis set. The negative values of $V_{S,min}$ were subsequently computed using the Wavefunction Analysis Program kindly provided by Bulat.[50] All molecular diagrams apart from the ORTEP one were drawn with PyMOL.[51]

Acknowledgements

The authors are grateful for funding from QREN-FEDER, through the COMPETE programme and FCT under project PTDC/QUI-QUI/101022/2008. FCT is acknowledged by M.S. and I.M for the PhD scholarships SFRH/BD/48490/2008 and SFRH/BD/87520/2012, respectively, and S.C. for the postdoctoral grant SFRH/BPD/42357/2007. We would also like to thank Dr. M. J. V. Brito for the assistance on the VT ^{1}H NMR experiments and Dr. Paula Branco from ASAE for the mass spectra.

Notes and references

[a] Departamento de Química, CICECO and iBiMED, Universidade de Aveiro, 3810-193 Aveiro, Portugal.
[b] Centro de Química e Bioquímica, DQB, Faculdade de Ciências, Universidade de Lisboa, Campo Grande, 1749-016 Lisboa, Portugal.

Electronic Supplementary Information (ESI) available: Electronic Supplementary data (ESD) available: ^{1}H and ^{13}C NMR spectra, as well as COSY, HMQC and HMBC correlation experiments of all compounds are included, except for **4** and **5**, for which only the ^{1}H NMR spectra are presented. The ^{1}H NMR titration data include the Job plots for **1** with ox^{2-}, (*S*,*S*)-$tart^{2-}$, fum^{2-} and $male^{2-}$ anions. Crystallographic and computational data are also included. See DOI: 10.1039/b000000x/

1. S. Kubik, in *Anion Coordination Chemistry*, eds. K. Bowman-James, A. Bianchi, and E. García-España, Wiley-VCH, Weinheim, 2012, pp 363-464.
2. G. R. Desiraju, *J. Am. Chem. Soc.*, 2013, **135**, 9952-9967.
3. E. R. D. Neta, S. D. Johanningsmeier, M. A. Drake and R. F. McFeeters, *J. Food Sci.*, 2009, **74**, S165-S169.
4. A. Munnich, *Nat. Genet.*, 2008, **40**, 1148-1149.
5. K. S. Oyedotun and B. D. Lemire, *J. Biol. Chem.*, 2004, **279**, 9424-9431.
6. U. R. G, R. Lo, S. Roy, T. Banerjee, B. Ganguly and A. Das, *Chem. Commun.*, 2013, **49**, 9818-9820.
7. W. Shaw, in *Biological Treatments for Autism and PDD*, Sunflower Pub, 3rd edition edn., 2008, pp. 23-42.
8. (a) P. Rustin, T. Bourgeron, B. Parfait, D. Chretien, A. Munnich and A. Rötig, *Biochimica et Biophysica Acta (BBA) - Molecular Basis of Disease*, 1997, **1361**, 185-197; (b) J.-J. F. J. G.-R. A.-P. R. P. Brière, *American Journal of Physiology - Cell Physiology*, 2006, **291**, C1114-C1120.
9. I. Baric, L. Wagner, P. Feyh, M. Liesert, W. Buckel and G. F. Hoffmann, *J. Inherit. Metab. Dis.*, 1999, **22**, 867-881.
10. (a) M. V. Dutton and C. S. Evans, *Can. J. Microbiol.*, 1996, **42**, 881-895; (b) J. Mandl, A. Szarka and G. Banhegyi, *Br. J. Pharmacol.*, 2009, **157**, 1097-1110.
11. J. G. Kelly, G. Doyle, J. Donohue, M. Laher, M. J. Vandenburg, W. J. Currie and W. D. Cooper, *Br. J. Clin. Pharmacol.*, 1986, **21**, 63-69.
12. J. W. Hainer and J. Sugg, *Vascular health and risk management*, 2007, **3**, 279-288.
13. W. J. Burke, *Expert opinion on investigational drugs*, 2002, **11**, 1477-1486.
14. A. J. Cutler, J. M. Goldstein and J. A. Tumas, *Clin. Ther.*, 2002, **24**, 209-222.
15. (a) C. Cruz, R. Delgado, M. G. Drew and V. Felix, *J. Org. Chem.*, 2007, **72**, 4023-4034; (b) K. Ghosh and A. R. Sarkar, *Tetrahedron Lett.*, 2009, **50**, 85-88; (c) C. Caltagirone and P. A. Gale, *Chem. Soc. Rev.*, 2009, **38**, 520-563; (d) P. A. Gale, *Chem. Soc. Rev.*, 2010, **39**, 3746-3771; (e) M. Belen Jimenez, V. Alcazar, R. Pelaez, F. Sanz, A. L. Fuentes de Arriba and M. C. Caballero, *Organic & Biomolecular Chemistry*, 2012, **10**, 1181-1185; (f) M. Wenzel, J. R. Hiscock and P. A. Gale, *Chem. Soc. Rev.*, 2012, **41**, 480-520; (g) P. Bose, R. Dutta and P. Ghosh, *Organic & Biomolecular Chemistry*, 2013, **11**, 4581-4584; (h) C. J. Haynes, S. N. Berry, J. Garric, J. Herniman, J. R. Hiscock, I. L. Kirby, M. E. Light, G. Perkes and P. A. Gale, *Chem. Commun.*, 2013, **49**, 246-248; (i) P. A. Gale, N. Busschaert, C. J. Haynes, L. E. Karagiannidis and I. L. Kirby, *Chem. Soc. Rev.*, 2014, **43**, 205-241; (j) P. A. Gale and C. Caltagirone, *Chem. Soc. Rev.*, 2014.
16. C. D. Gutsche, *Calixarenes. An Introduction*, The Royal Society of Chemistry, Cambridge, 2nd edn, 2008.
17. (a) J. Clayden, S. J. M. Rowbottom, M. G. Hutchings and W. J. Ebenezer, *Tetrahedron Lett.*, 2009, **50**, 3923-3925; (b) W. Maes and W. Dehaen, *Chem. Soc. Rev.*, 2008, **37**, 2393-2402; (c) M. X. Wang, *Chem. Commun.*, 2008, 4541-4551; (d) M. X. Wang, *Acc. Chem. Res.*, 2012, **45**, 182-195; (e) J. Thomas, L. Dobrzanska, K. Van Hecke, M. P. Sonawane, K. Robeyns, L. Van Meervelt, K. Wozniak, M. Smet, W. Maes and W. Dehaen, *Org Biomol Chem*, 2012, **10**, 6526-6536.
18. (a) D. X. Wang, Q. Y. Zheng, Q. Q. Wang and M. X. Wang, *Angew. Chem. Int. Ed. Engl.*, 2008, **47**, 7485-7488; (b) D. X. Wang and M. X. Wang, *J. Am. Chem. Soc.*, 2013, **135**, 892-897.
19. M. X. Wang and H. B. Yang, *J. Am. Chem. Soc.*, 2004, **126**, 15412-15422.
20. A. I. Vicente, J. M. Caio, J. Sardinha, C. Moiteiro, R. Delgado and V. Félix, *Tetrahedron*, 2012, **68**, 670-680.
21. J. M. Caio, T. Esteves, S. Carvalho, C. Moiteiro and V. Felix, *Org Biomol Chem*, 2014, **12**, 589-599.
22. (a) V. Amendola, L. Fabbrizzi and L. Mosca, *Chem. Soc. Rev.*, 2010, **39**, 3889-3915; (b) A. F. Li, J. H. Wang, F. Wang and Y. B. Jiang, *Chem. Soc. Rev.*, 2010, **39**, 3729-3745.
23. K. Hattori, H. Sajiki and K. Hirota, *Tetrahedron Lett.*, 2000, **41**, 5711-5714.
24. F. W. McLafferty and F. Tureek, 4th edn., University Science Books, Sausalito, California, USA, 1993.
25. R. N. Icke, B. B. Wisegarver and G. A. Alles, *Organic Synthesis, Collected Volumes III*, 1955, 723.
26. W. C. Shieh, S. Dell and O. Repic, *Org. Lett.*, 2001, **3**, 4279-4281.
27. Q.-Q. Wang, D.-X. Wang, H.-W. Ma and M.-X. Wang, *Org. Lett.*, 2006, **8**, 5967-5970.
28. (a) L. Fielding, *Tetrahedron*, 2000, **56**, 6151-6170; (b) P. Thordarson, *Chem. Soc. Rev.*, 2011, **40**, 1305-1323; (c) K. Hirose, *Journal of Inclusion Phenomena*, 2001, **39**, 193-209.
29. (a) Z. D. Hill and P. MacCarthy, *J. Chem. Educ.*, 1986, **63**, 162; (b) E. J. Olson and P. Buhlmann, *J. Org. Chem.*, 2011, **76**, 8406-8412.
30. C. Frassineti, S. Ghelli, P. Gans, A. Sabatini, M. S. Moruzzi and A. Vacca, *Anal. Biochem.*, 1995, **231**, 374-382.

31. T. Fox and P. A. Kollman, *The Journal of Physical Chemistry B*, 1998, **102**, 8070-8079.
32. D. A. Case, T. A. Darden, T. E. Cheatham III, C. L. Simmerling, J. Wang, R. E. Duke, R. Luo, R. C. Walker, W. Zhang, K. M. Merz, B. Roberts, S. Hayik, A. Roitberg, G. Seabra, J. Swails, A. W. Götz, I. Kolossváry, K. F. Wong, F. Paesani, J. Vanicek, R. M. Wolf, J. Liu, X. Wu, S. R. Brozell, T. Steinbrecher, H. Gohlke, Q. Cai, X. Ye, J. Wang, M.-J. Hsieh, G. Cui, D. R. Roe, D. H. Mathews, M. G. Seetin, R. Salomon-Ferrer, C. Sagui, V. Babin, T. Luchko, S. Gusarov, A. Kovalenkou and P. A. Kollman, *AMBER 12*, University of California, San Francisco, 2012.
33. (a) J. Wang, R. M. Wolf, J. W. Caldwell, P. A. Kollman and D. A. Case, *J. Comput. Chem.*, 2004, **25**, 1157-1174; (b) J. Wang, R. M. Wolf, J. W. Caldwell, P. A. Kollman and D. A. Case, *J. Comput. Chem.*, 2005, **26**, 114-114.
34. G. Trogdon, J. S. Murray, M. C. Concha and P. Politzer, *J. Mol. Model.*, 2007, **13**, 313-318.
35. Y. Ma, K. Gross, C. Hollingsworth, P. Seybold and J. Murray, *J. Mol. Model.*, 2004, **10**, 235-239.
36. (a) N. Busschaert, S. J. Bradberry, M. Wenzel, C. J. E. Haynes, J. R. Hiscock, I. L. Kirby, L. E. Karagiannidis, S. J. Moore, N. J. Wells, J. Herniman, G. J. Langley, P. N. Horton, M. E. Light, I. Marques, P. J. Costa, V. Félix, J. G. Frey and P. A. Gale, *Chem. Sci.*, 2013, **4**, 3036; (b) C. J. Haynes, N. Busschaert, I. L. Kirby, J. Herniman, M. E. Light, N. J. Wells, I. Marques, V. Felix and P. A. Gale, *Org Biomol Chem*, 2014, **12**, 62-72.
37. A. J. Green and P. L. Popelier, *J. Chem. Inf. Model.*, 2014, **54**, 553-561.
38. M. J. Frisch, G. W. Trucks, H. B. Schlegel, G. E. Scuseria, M. A. Robb, J. R. Cheeseman, G. Scalmani, V. Barone, B. Mennucci, G. A. Petersson, H. Nakatsuji, M. Caricato, X. Li, H. P. Hratchian, A. F. Izmaylov, J. Bloino, G. Zheng, J. L. Sonnenberg, M. Hada, M. Ehara, K. Toyota, R. Fukuda, J. Hasegawa, M. Ishida, T. Nakajima, Y. Honda, O. Kitao, H. Nakai, T. Vreven, J. A. Montgomery Jr, J. E. Peralta, F. Ogliaro, M. Bearpark, J. J. Heyd, E. Brothers, K. N. Kudin, V. N. Staroverov, R. Kobayashi, J. Normand, K. Raghavachari, A. Rendell, J. C. Burant, S. S. Iyengar, J. Tomasi, M. Cossi, N. Rega, J. M. Millam, M. Klene, J. E. Knox, J. B. Cross, V. Bakken, C. Adamo, J. Jaramillo, R. Gomperts, R. E. Stratmann, O. Yazyev, A. J. Austin, R. Cammi, C. Pomelli, J. W. Ochterski, R. L. Martin, K. Morokuma, V. G. Zakrzewski, G. A. Voth, P. Salvador, J. J. Dannenberg, S. Dapprich, A. D. Daniels, Ö. Farkas, J. B. Foresman, J. V. Ortiz, J. Cioslowski and D. J. Fox, *Gaussian 09, Revision A.01*, Gaussian, Inc., Wallingford CT, 2009.
39. D. D. Perrin and W. L. F. Armarego, *Purification of Laboratory Chemicals*, Butterworth-Heinemann, Oxford, 4th edn, 1996.
40. Bruker, *SAINT-plus*, (2007) Bruker AXS Inc., Madison, Wisconsin, USA.
41. G. M. Sheldrick, *SADABS*, (1996) University of Göttingen, Göttingen, Germany.
42. G. M. Sheldrick, *Acta Crystallogr. A*, 2008, **64**, 112-122.
43. O. V. Dolomanov, L. J. Bourhis, R. J. Gildea, J. A. K. Howard and H. Puschmann, *J. Appl. Crystallogr.*, 2009, **42**, 339-341.
44. C. I. Bayly, P. Cieplak, W. Cornell and P. A. Kollman, *J Phys Chem-Us*, 1993, **97**, 10269-10280.
45. F. H. Allen, *Acta crystallographica. Section B, Structural science*, 2002, **58**, 380-388.
46. (a) R. Salomon-Ferrer, A. W. Götz, D. Poole, S. Le Grand and R. C. Walker, *J. Chem. Theory Comput.*, 2013, **9**, 3878-3888; (b) A. W. Gotz, M. J. Williamson, D. Xu, D. Poole, S. Le Grand and R. C. Walker, *J. Chem. Theory Comput.*, 2012, **8**, 1542-1555; (c) S. Le Grand, A. W. Götz and R. C. Walker, *Comput. Phys. Commun.*, 2013, **184**, 374-380.
47. J.-P. Ryckaert, G. Ciccotti and H. J. C. Berendsen, *J. Comput. Phys.*, 1977, **23**, 327-341.
48. T. Darden, D. York and L. Pedersen, *J. Chem. Phys.*, 1993, **98**, 10089.
49. D. R. Roe and T. E. Cheatham, *J. Chem. Theory Comput.*, 2013, **9**, 3084-3095.
50. (a) F. A. Bulat and A. Toro-Labbe, *WFA: A suite of programs to analyse wavefunctions*, unpublished; (b) F. A. Bulat, A. Toro-Labbe, T. Brinck, J. S. Murray and P. Politzer, *J. Mol. Model.*, 2010, **16**, 1679-1691.
51. *The PyMOL Molecular Graphics System*, Version 1.3, Schrödinger, LLC.